HHS Public Access

Author manuscript

Biomaterials. Author manuscript; available in PMC 2019 September 01.

Published in final edited form as:

Biomaterials. 2018 September ; 177: 88–97. doi:10.1016/j.biomaterials.2018.05.038.

A Novel Lipidoid-MicroRNA Formulation Promotes Calvarial Bone Regeneration

Lei Sui[1,2], **Ming Wang**[3], **Qianqian Han**[1], **Liming Yu**[1], **Lan Zhang**[1], **Leilei Zheng**[1], **Junxiang Lian**[1], **Jin Zhang**[4], **Paloma Valverde**[1], **Qiaobing Xu**[5], **Qisheng Tu**[1,*], and **Jake Chen**[1,6,*]

[1]Division of Oral Biology, Tufts University School of Dental Medicine, Boston, MA, USA

[2]Department of Prosthodontics, Tianjin Medical University School and Hospital of Stomatology, Tianjin, China

[3]Beijing National Laboratory for Molecular Sciences, Key Laboratory of Analytical Chemistry for Living Biosystems Institute of Chemistry, Chinese Academy of Sciences (ICCAS), Beijing 100190, China

[4]Shangdong University, School of Stomatology, Jinan, Sangdong, China

[5]Department of Biomedical Engineering, Tufts University, 4 Colby Street, Medford, MA, USA

[6]Department of Anatomy and Cell Biology, Tufts University School of Medicine, Sackler School of Graduate Biomedical Sciences, Boston, MA, USA

Abstract

Specific microRNAs (miRs) and the Wnt signaling pathway play critical roles in regulating bone development and homeostasis. Our previous studies revealed the ability of miR-335-5p to promote osteogenic differentiation by downregulating Wnt antagonist Dickkopf-1 (DKK1). The purpose of this study was to use nano-materials to efficiently deliver miR-335-5p into osteogenic cells for tissue engineering applications. We synthesized and screened a library of 12 candidate nano-lipidoids, of which L8 was identified as the preferred biodegradable lipidoid for miRNA molecule delivery into cells. We then investigated whether a lipidoid-miRNA formulation of miR-335-5-p (LMF-335) could successfully deliver miR-335-5-p into cells to promote osteogenesis *in vitro* and calvarial bone healing *in vivo*. Transfection of C3H10T1/2 cells and bone marrow stromal cells (BMSCs) with LMF-335 led to decreased expression of DKK1 and increased expression of the key osteogenic genes. LMF-335 and LMF-335-transfected BMSCs were then used in combination

*Address all correspondence and reprint requests to Jake Chen, DMD, MDS, PhD, Tufts University School of Dental Medicine, One Kneeland Street, DHS-643, Boston, MA 02111; Tel: (617) 636-2729; Fax: (617) 636-0878; jk.chen@tufts.edu, Qisheng Tu, M.D., Ph.D., Tufts University School of Dental Medicine, 1 Kneeland Street, DHS-638, Boston, Massachusetts 02111, USA. Telephone: 617-636-2937; Fax: 617-636-0878; qisheng.tu@tufts.edu.

Conflicts of interest

The authors declare no competing financial interest.

Data Availability Statement

The raw/processed data required to reproduce these findings cannot be shared at this time due to technical or time limitations.

with silk scaffolds to evaluate healing of critical-size calvarial bone defects in mice. The results revealed significant new bone formation in the defects in LMF-335 groups as compared with control groups. In conclusion, this first report supports the notion that lipidoid delivery of miRNA can be used to induce osteogenic differentiation of stem cells and bone regeneration.

Graphical abstract

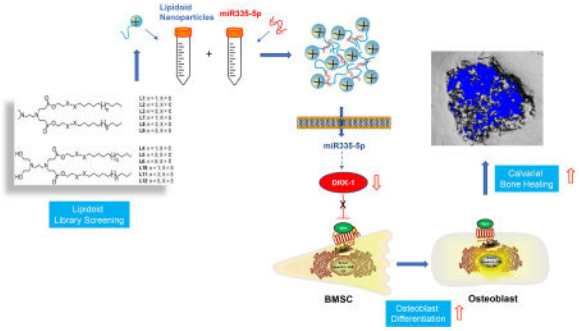

Keywords

Lipidoid; microRNA; miR-335-5p; Bone marrow stromal cells (BMSCs); Osteogenic Differentiation; Bone Formation

1. Introduction

Reconstruction of damaged, diseased, or congenitally missing craniofacial bones is constantly a challenge for craniofacial surgeons. Suitable replacement materials for craniofacial defects include autografts, allografts, and scaffolds for tissue regeneration such as metal and polymers. Despite autografts providing the best clinical outcome, they are associated with low availability and donor site damage. Allografts, on the other hand, frequenty lead to poor quality outcomes, high risk of disease transmission and high costs. Consequently, a variety of scaffolds has been commonly used in the clinic and tremendous efforts have been devoted to improving osteogenesis on these scaffolds, including enhancing the biocompatibility of scaffold materials [1], utilizing stem cells or iPSC [2], and administering various growth factors. These tissue engineering approaches are promising applications to tissue regeneration in other regions, with the hope that they will facilitate restoration of missing functions during the process of regeneration and subsequent integration with the host tissue [3].

The induction of osteogenesis is a carefully orchestrated process that involves transcriptional and post-transcriptional gene expression regulation [4–8]. Post-transcriptional regulation has been shown to quickly alter target protein levels through controlling the existing mRNAs [9]. Consequently, a rapid osteogenic gene expression may be effected on bone defect sites when the post-transcriptional regulation mechanism is triggered by specific bioactive molecules, which would, in turn, improve the bone healing process of critical sized defects.

MicroRNAs (miRNAs) are an abundant class of ~22-nucleotide (nt) double-stranded noncoding RNAs that are considered key post-transcriptional regulators of gene expression [10, 11]. By base pairing with specific sequences on the 3'-UTR of target mRNAs, miRNAs induce either translational repression or cleavage of targeted mRNAs [12]. Hence, they provide a potential therapeutic strategy for rapid fine-tuning of gene expression. Indeed, miRNA-based therapeutics has already entered Phase 2a clinical trial [13].

In a previous study, we identified and characterized a novel miRNA, miR335-5p, which specifically targets the 3'-UTR sequence of DKK1 and regulates its gene expression [14]. Functional analysis revealed that miR335-5p is an important regulator of osteogenic differentiation and is critical in maintaining the osteogenic capacity of bone forming cells. In a more recent study we demonstrated specific overexpression of miR-335-5p driven by an osterix promoter in the osteoblast lineage induces osteogenic differentiation and bone formation in mice, supporting the potential application of miR-335-5p-modified BMSCs in craniofacial bone regeneration [15]. Despite the potential of miR-335-5p to induce bone formation *in vivo*, developing an efficient and cost-effective delivery technique to reconstruct bone defects is still a clinical challenge.

A variety of cationic lipid-like materials, termed lipidoids, has emerged as a promising gene delivery platform, by taking advantage of a combinatorial synthesis strategy to identify the most efficient delivery nanocarriers. Lipidoids can form spherical nanoparticles with a size of 300nm, encapsulate genes via electrostatic interactions and form nanoparticles for delivery of various biomacromolecules including plasmid DNA, mRNA, siRNA and proteins [16–24]. The high efficiency and safety of lipidoids as a gene delivery platform could potentially be used for in vivo delivery of miRNA including miR335-5p to induce bone regeneration. The current paper describes the development and the first attempt to apply lipidoid-miRNA335-5p formulation (LMF-335) to promote craniofacial bone regeneration. We synthesized a combinatorial library of candidate lipidoids and performed a library screening to achieve optimal intracellular miRNA delivery through in vitro assay. Once the most suitable candidate lipidoid was identified, we characterized the optimal lipidoid-miRNA ratio of conjugation. We then investigated the *in vitro* and *in vivo* effects of LMF-335 transfection on the differentiation of stem cells toward the osteogenic lineage and on enhancing calvarial critical-size defect healing in a murine model.

2. Materials and methods

2.1. Synthesis of candidate lipidoids and nanoparticulate vectors

All lipidoids used in this study (Figure 1) were synthesized using Michael addition conjugation as previously described [25, 26]. We formulated lipidoid nanoparticles for miRNA delivery, by mixing lipidoids, cholesterol (purchased from Sigma-Aldrich Cat. # C8667), and 1, 2-dioleoyl-*sn*-glycero-3-phosphoethanolamine (DOPE) in chloroform at weight ratios of 16:4:1, followed by chloroform evaporation under vacuum. The resulting thin film was then rehydrated with PBS to obtain lipidoid nanoparticulate vectors at a concentration of 1 mg/mL.

2.2. Sequences of miRNA335-5p mimics and negative controls

Ambion® miRNA335-5p mimics (Sequence: UCAAGAGCAAUAACGAAAAAUGU) and miRNA333-5p inhibitors (Sequence: GGAUGAUUGCUGACGUGGATT), as well as their negative controls (NC) (validated, non-targeting siRNA sequences), were purchased from Life Technologies (Carlsbad, CA, USA). The miRNA mimic is a synthetic, double-stranded LNA-based oligonucleotide with a guide strand that is identical to the miRNA and a passenger strand containing stabilization and uptake elements such as cholesterol. The miRNA inhibitor is a small, chemically modified single-stranded RNA molecules designed to specifically bind to and inhibit endogenous miRNA molecules and enable miRNA functional analysis by down-regulation of miRNA activity. The LMFs were prepared using the selected optimal lipidoid at the lipidoid/miRNA ratio of 5:1, and transfection was carried out twice within a time span of 2 days.

2.3. Animal maintenance

Six- to eight-week-old male C57BL/6J mice were purchased from the Jackson Laboratory (Bar Harbor, ME, USA) and routinely acclimated for one week in the animal facility at Tufts–New England Medical Center before initiation of experimental procedures. Mice were maintained according to the Guide for the Care and Use of Laboratory Animals, recommended by the Institute of Laboratory Animal Resources, National Research Council (DHHS Publ. NIH 86-23, 1985). The experimental protocol was approved by the Institutional Animal Use and Care Committee at the Tufts–New England Medical Center.

2.4. Cell culture

C3H10T-1/2 cells were cultured in Dulbecco's modified Eagle medium (DMEM) (Life Technologies, Rockville, MD) supplemented with 10% fetal bovine serum (FBS), 100U/mL of penicillin and 100mg/mL of penicillin-streptomycin. Primary murine bone marrow stromal cells (BMSCs) were obtained from femurs and tibias of 6- to 8-week-old male C57BL/6J mice and cultured in DMEM supplemented with 20% FBS, 1% penicillin-streptomycin as previously described [27]. Fifty mg/mL of ascorbic acid (Sigma, USA) and 10nM dexamethasone (Sigma, USA) was added to the culture medium to induce osteogenic differentiation before transfection. Culture medium was replaced by antibiotic-free fresh medium 24 h before transfection. Cells were allowed to reach 70%–80% confluency prior to transfection analysis.

2.5. Transfection and flow cytometry analysis

To identify the optimal lipidoid/miRNA ratio, a Cy3-labeled miRNA NC (Ambion, Life Technologies, USA) was used, and nanoparticle formulations generated by diluting miRNA mimics and different amount of lipidoid L1 with 200μL of sodium acetate buffer solutions (NaOAc) (25mM, pH = 5.5). The lipidoids at different concentrations were added to 100pmol (1.41μg) miRNA NaOAc solution at room temperature. After brief vortexing, the mixture was allowed to stand for 15min to form LMFs. For each transfection experiment, Cy3-labeled LMFs were added to C3H10T1/2 cell monolayers at a final concentration of 30 nM miRNA in antibiotic-free and serum-free medium, and the control group was treated with free Cy3-labeled miRNA negative control. After 6 h incubation, transfected cells were

harvested by trypsin, washed with phosphate buffered saline (PBS), and fixed in 1% paraformaldehyde in PBS for evaluation on a flow cytometer (LSR-II; BD Biosciences, San Jose, CA). Ten thousand cellular events were gated using forward, and side scatter settings. Gating was determined with control cells. The geometric mean of this population in the PerCP-Cy3 channel was used as a measure of Cy-3 fluorescence. Three parallel samples were tested for each group, and results analyzed using FlowJo 6.1.1 software (Tree Star Inc., San Carlos, CA) as previously described [28]. The transfection efficiency was represented as the percentage of fluorescence positive cells, and the optimal lipidoid/miRNA ratio was then determined. Cy3-labeled miRNA NC was later complexed with L1 to L12 candidate lipidoids at 5:1 ratio and compared with commercially available transfection agent Lipofectamine 2000 (Invitrogen, USA). The nanoparticle complexes were added to C3H10T1/2 cells at a final concentration of 30nM miRNA.

2.6. Cell proliferation assays

Cell Counting Kit-8 (CCK-8; Dojindo, Gaithersburg, MD) was used to monitor cell proliferation according to the manufacturers' instructions. C3H10T1/2 cells were seeded into 96-well tissue culture plates at a density of 5000 cells per well and transfection was carried out 24 h later with 12 candidate LMFs at the lipidoid/miRNA-335-5p mimics ratio of 5:1. Media aliquots were collected at 12 h and every 24 h after transfection for cell viability detection. Briefly, the culture medium was removed, and the cultures were washed with PBS twice. Then 100μL of serum-free medium and 10μL of CCK-8 were added to each well, followed by incubation at 37°C for 3h. The supernatant was transferred to a new 96-well plate, and the absorbance at 450nm was measured using a spectrophotometer (Biotek, Winooski, VT). The experiment was performed in triplicate.

2.7. Cytotoxicity assays

Cytotoxicity of the LMFs was assessed by evaluating release of cellular lactate dehydrogenase (LDH) as a marker of cell membrane integrity disruption. C3H10T1/2 cells were cultured and treated with 12 candidate LMFs as previously described. After 6, 12, 24, 48 and 72h post-transfection, media were collected, centrifuged to settle the cells, and then assayed for cellular LDH using an LDH-Cytotoxicity Assay Kit II (Abcam, Cambridge, MA). The LDH activities from different time points were determined spectrophotometrically according to the manufacturer's recommendations. High-toxicity controls were included by incubating cells with 1% Cell Lysis Solution. Experiments were performed in triplicate.

2.8. Particle size detection

The particle size of both free L8 lipidoid and miRNA mimics-loaded LMF was determined with a Dynamic Light Scattering (DLS) detector and previously described [25, 26].

2.9. Fluorescence microscopic examination

C3H10T1/2 cells grown in a chamber slide system (Nunc, Naperville, IL, USA), transfected and analyzed by fluorescence microscopy as previously described [28]. Briefly cells were transfected with Cy3-labeled miRNA/L8 LMF complexes, and then fixed with 4% paraformaldehyde at 6 h post-transfection. Cell nuclei were stained with DAPI. Images were

captured using an OLYMPUS BX53 fluorescence microscopy with Cellsens digital image software (Olympus, Center Valley, PA, USA).

2.10. RNA isolation and qRT-PCR analysis

Total RNA was isolated from cultured cells by using the RNeasy Plus Mini kit (Qiagen, Valencia, USA) as per manufacturer's instructions. Total RNA isolation from tissues was performed with the TRIzol solution (Invitrogen, CA, USA) as recommended by the manufacturer. Quantitative real-time reverse-transcriptase PCR (qRT-PCR) assay was performed using SYBR Green Supermix (Bio-Rad Laboratories, Hercules, CA, USA) on a Bio-Rad iQ5 thermal cycler (Bio-Rad Laboratories). Gene expression data were normalized to GAPDH by the comparative cycle threshold (CT) method. Primers used for amplification are listed in Table 1.

2.11. Western blot analysis

Whole protein cell lysates were prepared as described previously [29] and protein concentration determined using the BCA Protein Assay Reagent Kit (Bio-Rad, Hercules, CA, USA). Protein samples were subjected to electrophoresis on 10% Tris-glycine premade gels (Bio-Rad) and transferred to nitrocellulose membranes (Bio-Rad) by immunoblotting. After 1h blocking in 5% (wt/vol) nonfat skim milk at room temperature, membranes were incubated at 4°C overnight in TBS-T containing the following antibodies (Santa Cruz, CA, USA): DKK1 (1:10000); Osx (1:10000); Runx2 (1:10000); Satb2 (1:10000). Membranes were then incubated with horseradish peroxidase–labeled goat-anti-rabbit secondary antibodies (Santa Cruz, CA, USA) for 90min at room temperature. Blots were visualized with electrogenerated chemiluminescence (ECL) chemiluminescence detection (Pierce, Rockford, IL, USA). Scanning densitometry was performed with ImageJ image analysis software as previously described [29].

2.12. Calvarial bone regeneration in mice

After anesthesia, two critical-sized calvarial defects with a diameter of 4-mm were created on both sides of the calvarial bone using a low-speed dental bur with saline raise. Care was taken to minimize invasion of the Dura mater which contributes significantly to calvarial bone healing process. Then the cylinder-shaped SS with 4-mm-diameter and 2-mm-thickness was gently placed in the defect gently using tissue forceps. To investigate the role of LMF335 in calvarial bone defect healing animals were were randomly assigned into four groups of 7 defects each, receiving the following treatments: (1) empty silk scaffold (SS) implantation; (2) SS seeded with BMSCs (SS-BMSCs) implantation; (3) empty SS implantation followed by LMF-335 local injection (SS-LMF-injection); (4) SS seeded with LMF-335-transfected BMSCs (SS-LMF-BMSCs) implantation. For the SS-LMF-injection group, LMF-335 was injected subcutaneously to the scaffold region twice weekly for four weeks, beginning from the surgery day. For the SS-LMF-BMSCs group, BMSCs were transfected with LMF-335 twice, at two days and five days before surgery. LMF-335-transfected BMSCs were concentrated to 2×10^7 cells/mL in medium, and then seeded onto the silk scaffold by pipetting the cells suspension onto the materials. The BMSCs/SS construct was incubated for an additional 4 h to enable cell attachment ex vivo prior to

implantation. Three mice were sacrificed for each group five weeks after surgery, and the cranial samples were frozen immediately in liquid nitrogen and kept at −80°C for qRT-PCR.

2.13. Micro-computed tomography (μCT) analysis

Five weeks post-surgery, mice were euthanized, and calvarial bones collected. Healing of calvarial bone defects was evaluated with a μCT system Scanco μCT40, SCANCO Medical AG, Brüttisellen, Switzerland) as previously described [30]. All samples were processed under kVP of 300 V, one mA and exposure time of 0.8s. The morphology of reconstructed calvarial bone was assessed using the micro-CT settings reported previously, and the images were segmented using a nominal threshold value of 300 to perform a three-dimensional (3D) histomorphometric analysis. The bone defect healing was compared with parameters of bone volume fraction (bone volume/total volume, BV/TV), volume of newly regenerated bone, and density of bone volume (DBV) was used for comparison.

2.14. Histology and immunohistochemical staining protocols

Cranial bone samples were processed for histology and immunohistochemical staining for osteocalcin (OCN) expression as previously described [15, 30]. H&E staining and immunostaining sections were examined and photographed with an OLYMPUS BX53 fluorescence microscopy with Cellsens digital image software (Olympus, Center Valley, PA, USA). Newly formed bone was quantified in 4 sections of at least 4 different defects per animal group as previously described [27, 31]. New bone formation on each section was expressed as a percentage of the total area of the defect.

2.15. Statistical analysis

Experimental data were expressed as mean ± standard deviation. Statistically significant differences ($p<0.05$) between groups were analyzed using the one-way ANOVA method followed by appropriate posthoc tests (Dunnett's or Tukey's HSD). Statistical analyses were performed using an SPSS 16.0 (SPSS Inc., Chicago, IL, USA) software package.

3. Results

3.1. In vitro screening of LMFs for miRNA delivery

To develop the optimal formulation of LMFs for miRNA delivery, lipidoid L1 and Cy3-labeled miRNA NC were mixed at various lipidoid:miRNA weight ratios. We then compared the transfection efficacy of different LMF formulations in C3H10T1/2 cultures via flow cytometry, using free miRNA as a negative control. As shown in Figure 2A, all LMFs except those developed at 1:2 lipidoid/miRNA ratio demonstrated significantly higher transfection efficiency than the control group. The highest transfection efficiency was achieved at the lipidoid/miRNA ratio of 5:1 and 7:1. To minimize cytotoxicity associated with transfection reagents, we selected a 5:1 lipidoid/miRNA ratio in subsequent experiments.

We then investigated the transfection efficiencies for LMFs generated with 12 lipidoids (Figure 2B) by calculating the percentage of transfected cells with fluorescence intensities above nontransfected cells by flow cytometry analysis. LMFs generated with lipidoids L2, L3, L4, L6, L8 and L12 exhibited a similar or higher transfection efficiency than

Lipofectamine 2000, a commercially available tranfection reagent used as a positive control. Among all LMFs, L3 demonstrated the best transfection efficiency (Figure 2B) with a value of 87.2±8.3%. Whereas LMFs generated with lipidoids L2, L4, L6, L8, L9, L10, and L12 led to transfection efficiencies higher than 50%, those produced by L1, L5, L7, and L11 had lower than 50% transfection efficiency.

CCK-8 assays were then implemented to investigate the putative anti-proliferative effects of LMFs on C3H10T1/2 cells (Figure 3A). All LMFs decreased cell proliferation significantly however, the inhibitory effects were not uniform among formulations. Thus, LMFs derived from non-biodegradable lipidoids (L1 to L6) affected proliferation in lower extent than most of the biodegradable lipidoids (L7 to L12), with the exception of biodegradable L8, L9, and L12 that achieved comparable results than non-biodegradable ones.

We then measured LDH release from C3H10T1/2 cells to evaluate LMFs cytotoxicity (Figure 3B). Results revealed significant LDH release after LMFs exposure for 6 and 12 h. This suggested interaction of LMFs with the cell membrane during endocytic processes could compromise the integrity of the cell membrane. However, the toxic response reached a plateau stage after 12 h, probably resulting from a rapid recovery of the cell membrane. In general, LMFs derived from biodegradable lipidoids exhibited higher cytotoxicity than non-biodegradable ones, with the exception of L8 and L9 that led to comparable cytotoxicity as non-biodegradable lipidoids, with the exception of L2.

We compared the cytotoxicity and influence of L8 formulation on cell proliferation with Lipofectamine 2000. No statistically significant difference was observed (Supplement Fig 1). To determine whether LMF-335 induces inflammatory cytokine production, we have detected the expressions of inflammatory cytokines after BMSCs were transfected with LMF-335 following seven days of incubation with ascorbic acid and dexamethasone. The results showed that no significant difference was found in the expressions of IL-1β, IL-10 and TNF-α after the cells received lipdoid-miRNA transfection (Supplemental Fig 2). Similar results were observed for interferon β and interferon γ expressions (data not shown). Based on transfection efficiency values, biodegradability properties, and lowest effects on cell proliferation and cytotoxicity, L8 was selected as the preferred lipidoid for delivery of miRNA335-5p in our study.

3.2. Intracellular uptake of LMFs

LMFs were then developed with Cy3-labeled miRNA with either L8 or Lipofectamine 2000 and used to transfect C3H10T1/2 for 6 h to visualize intracellular delivery of miRNA into the cells. Microscopic examination revealed bright yellow fluorescence due to Cy3-labeled miRNA distributed in the cytoplasm but not in the nuclei (Fig. 4). Furthermore, there were more intracellullar fluorescence bursts observed in L8 group than in Lipofectamine 2000 group (Fig. 4).

3.3. Evaluation of LMFs particle size by DLS

We then evaluated the hydrodynamic sizes of free L8 lipidoid and LMFs nanoparticles at 5:1 lipidoid/miRNA ratio by DLS. Both free lipidoid L8 and LMFs formed narrowly distributed

nanoparticles. Whereas the diameter of free L8 lipidoid nanoparticles was 277.6±7.9 nm, the diameter increased significantly to 346.7±6.1 nm when loaded with miRNA335-5p.

3.4. Evaluation of LMF-335 osteogenic effects *in vitro*

In previous reports, we demonstrated that miRNA335-5p can promote osteogenesis *in vitro* [14] and *in vivo* [15]. To determine whether lipidoid-miRNA335-5p (LMF-335) nanoparticles could be used to deliver miRNA335-5p into cells and bone defects and induce osteogenesis, C3H10T-1/2 cells and BMSCs were transfected twice with LMF-335 following seven days of incubation with ascorbic acid and dexamethasone. Transfection experiments were performed in parallel with LMFs of miRNA mimic NC (mNC), miRNA inhibitor negative control (iNC), miR335-5p mimic (335) and miR335-5p inhibitor (335i). We then evaluated gene expression of osteogenic markers including BSP, Osx, Runx2, and Satb2 48 hours after the second transfection. Whereas none of the NCs mediated significant effects, LMF-335 increased the gene expression of BSP by 3-fold ($P < 0.01$), Osx and Runx2 by over 2-fold ($P < 0.05$), and Satb2 by almost 2-fold ($P < 0.05$) in C3H10T-1/2 cells. LMF-335 led to similar upregulation pattern when transfected into BMSC, with the highest effects on BSP and the lowest on Satb2 expression (Fig. 5).

Western blot analysis revealed that LMF-335 affected protein expression of Osx, Runx2, and DKK1 in C3H10T-1/2 (Figure 6A) and BMSCs (Figure 6B). In agreement with osteogenic-upregulation by LMF-335 through DKK1 downregulation, Osx and Runx2 protein expression in LMF-335-treated cells were higher than in control cells wherea DKK1 expression was significantly downregulated. LMF generated with miR335-5p inhibitor (335i) increased DKK1 protein expression and decreased that of Runx2 and Osx (Figure 6) whereas the other LMF negative controls did not mediate any significant effect.

3.5. Calvarial bone healing induced by LMF-335

We then compared the capacity of LMF-335 injected locally and BMSCs transfected with LMF-335 to regenerate critical-sized defects (4 mm in diameter) created on each side of the calvarial bone. BMSC were transfected twice, the first transfection was performed 5 days before surgery, while the second transfection was performed 2 days before surgery. According to μCT analysis, the ratio of BV to TV was significantly higher in defects injected locally with LMF-335 or repaired with BMSCs transfected with LMF-335 than in the empty silk scaffold group or the one repaired with untransfected BMSCs (Figure 7, $P<0.05$).

Histological analysis of repaired defects revealed locally injected LMF-335 and LMFs-transfected BMSCs filled the defect with new bone areas whereas whereas the control groups led to the formation of fibrous connective tissues and minimal new bone formation areas scattered across the defect (Figure 8, $P<0.05$). The ratio of newly formed bone to total defect area was significantly higher in the locally injected and LMF-335-transfected group that in the control groups (Figure 8, $P<0.05$). Further immunohistochemical staining with an OCN antibody demonstrated higher OCN expression levels in defects regenerated with locally injected LMF-335 and LMF-transfected BMSC as compared with control groups (Figure 8, $P<0.05$).

4. Discussion

The human body is capable of repairing minor bone defects, but when it comes to a critical-sized bone defect, the repair is challenging. The existing materials and techniques for craniofacial defects reconstruction have disadvantages including infection, rejection, the limited supply, pain, function compromising. With the recent development of new materials and gene therapy, tissue engineering has become one of the most promising therapeutic approaches to repair bone defects. Promoting osteogenic gene expression at bone defect sites could be used to improve the bone healing process. We hypothesized that the targeted knock down of genes through miRNA mimics pairing with specific sequences in the 3'-UTR of target mRNA could activate osteogenesis and healing on the calvarial defect sites. Previous studies have shown miRNA335-5p as a promising therapeutic target to promote bone formation and regeneration partly by downregulating DKK1, then reducing the inhibitory effect on Wnt-signal and increasing expression of key osteogenic genes, Runx2, bone sialoprotein (BSP) and osterix (OSX) [14].

However, RNAi effectors are unable to reach cells without the assistance of a delivery system or vector. Thus, developing a novel technique to deliver osteogenic miRNA is an innovative and clinically relevant challenge. Currently, either optimal viral or synthetic delivery system remains limited, in part because of their cytotoxic effects, relatively higher immunogenicity and slow, multi-step syntheses. Earlier reports revealed some of the advantages of using novel intracellular delivery materials, a new class of lipid-like delivery molecules lipidoids. The straightforward and economic combinatorial synthesis of lipidoids together with their high delivery efficiencies makes them a new promising class of non-viral delivery vectors for therapeutic applications. Prior studies demonstrated successful silencing using lipidoids both *in vitro* and *in vivo* [20], [21], [22, 32]. Hence, we employed this promising nanocarrier to create a lipidoid-miRNA335-5p formulation (LMF-335) to deliver functionally active miRNA335-5p into cultures of both murine mesenchymal stem cell-like C3H10T1/2 cells and primary bone marrow stem cells (BMSCs), aiming to target DKK1 gene. As far as we know, our study is one of the first reports demonstrating efficacy of lipidoids-delivered miRNA to induce craniofacial bone healing [23, 24, 33].

Lipidoids were prepared by heating commercially available amines with lipophilic acrylates, without solvent or catalysts, according to our previously reported methods [20]. Lipidoid nanoparticles were formulated with DOPE in current study, because a previous study demonstrated DOPE could facilitate endosomal escape and gene transfection [26]. Once we identified the optimal Lipidoid/miRNA ratio (5:1) in initial screening experiments with L1 lipidoid, flow cytometry experiments revealed 67% of lipidoids generated exhibited comparable or higher transfection efficiency than Lipofectamine 2000 used as a positive control. Among the biodegradable lipidoids used in this study, L8 exhibited one of the highest transfection efficiency (almost 85%) and led to lower cytotoxicity but not lower cell proliferation as compared with non-biodegradable lipidoids. Besides, we didn't observe the effect of miRNA delivery using LMF-335 on inflammatory cytokine production. The positive charges in the NP of LMF will increase when lipidoid:miRNA ratio increases. This is because the LMFs will better attach to the cell membrane and then get into the cell, so the

transfection efficiency increases. Because of different chemical structures, LMFs have different abilities to interact with cell membranes as well as cargo molecules.

It is proven that compared with commercially Lipofectamine 2000, lipidoids formed narrowly distributed nanoparticles and easier control of their molecular composition, simplified manufacturing, modification and analysis, tolerance for cargo size. When we evaluated intracellular uptake of of Cy-3 labeled miRNA by L8 LMFs or Lipofectamine 2000 in C3H10T1/2 cells, we found fluorescence assocated with intracellular miRNA intake in the cytoplasm, but not in the cell nuclei and L8 LMFs exhibited a much higher transfection efficiency than Lipofectamine 2000. In vitro transfection experiments with both murine mesenchymal stem cell-like C3H10T1/2 cells and primary BMSCs using previously selected optimal lipidoid L8 at the lipidoid/miRNA ratio of 5:1, LMF-335-treated cells significantly increased approximately 2–3 folds compared to control at level of osteogenic transcription factors and protein expression. Thes results supported our hypothesis that LMF-335 could deliver miRNA into the cytoplasm, target and downregulate DKK1 gene in Wnt signaling pathway, promoting osteogenic differentiation. To evaluate whether LMF-335 could also promote osteogenic differentiation and bone regeneration in vivo we examined calvarial bone defect healing resulting from locally injecting LMF-335 or implanting LMF-335 transfected BMSCs into the bone defects. In cranial bone, repair and regeneration is dependent upon the adjacent periosteum and dura. In this case, a silk scaffold (SS) was used to direct the migration and enhancement of the proliferation/differentiation of osteoprogenitor cells on the defect sites [34]. We then systematically evaluated the ability of LMF-335 to enhance BMSCs osteogenesis, and the therapeutic potential of LMF-335 modified BMSCs to regenerate mouse calvarial bone defects. We found that LMF-335 dramatically improved the craniofacial reconstruction, as evidenced by increased bone volume and increased bone mineral density *in vivo*.

We previously reported that transgenic mice overexpressing miR-335-5p [15] constitutively exhibited a downregulation in DKK1 expression and upregulation of beta-catenin, which correlated with increased bone formation in transgenic mice as compared with wild-type littermates. In that study, BMSC isolated from the transgenic mice had higher potential to regenerate calvarial bone than BMSC isolated with wild-type mice.

BMSC transfected twice with LMF-335 and then implanted into craniofacial bone defects, led to more than 3-fold higher BV/TV than any of control groups including the LMF-mNC-transfected BMSC group or the LMF-mNC local injection delivery group. Local injection of LMF-335 increased BV/TV more than 5-fold. In our previous transgenic study, we also found BMSC isolated from transgenic mice overexpressing miR-335-5p constitutively drove 4-fold higher BV/TV than BMSC isolated from wild-type littermates [15]. In both craniofacial regeneration studies subtle downregulation in DKK1 protein expression in the BMSC correlated with increased craniofacial bone regeneration. When new bone formation areas were evaluated by HE and OCN analysis, we found ~2-fold increase in new bone (BV/TV%) and ~2-fold increase in OCN expression in the LMF-335-transfected BMSC group compared to the control groups. Previously, we also found similar fold-increases in new bone formation areas and OCN upregulation when regenerated craniofacial bone

defects from transgenic mice overexpressing miR-335-5p and wild-type littermates were compared [15].

Taken together, our experimental results support the notion that LMF-335 can promote osteogenesis *in vitro* and *in vivo*. Therefore lipidoid delivery of miR-335-5p could potentially be used to induce osteogenic differentiation of stem cells and calvarial bone regeneration.

Supplementary Material

Refer to Web version on PubMed Central for supplementary material.

Acknowledgments

This work was supported by R01DE021464 and R01DE025681 through the National Institutes of Health and an Innovation in Oral Care Award through International Association for Dental Research and GlaxoSmithKline Consumer Healthcare, and an Award through International Team of Implantology to JC.

References

1. Thein-Han WW, Saikhun J, Pholpramoo C, Misra RD, Kitiyanant Y. Chitosan-gelatin scaffolds for tissue engineering: physico-chemical properties and biological response of buffalo embryonic stem cells and transfectant of GFP-buffalo embryonic stem cells. Acta biomaterialia. 2009; 5:3453–66. [PubMed: 19460465]
2. Ye JH, Xu YJ, Gao J, Yan SG, Zhao J, Tu Q, et al. Critical-size calvarial bone defects healing in a mouse model with silk scaffolds and SATB2-modified iPSCs. Biomaterials. 2011; 32:5065–76. [PubMed: 21492931]
3. Langer R, Vacanti JP. Tissue engineering. Science (New York, NY). 1993; 260:920–6.
4. Zaidi SK, Young DW, Montecino M, van Wijnen AJ, Stein JL, Lian JB, et al. Bookmarking the genome: maintenance of epigenetic information. The Journal of biological chemistry. 2011; 286:18355–61. [PubMed: 21454629]
5. Sohn YD, Somasuntharam I, Che PL, Jayswal R, Murthy N, Davis ME, et al. Induction of pluripotency in bone marrow mononuclear cells via polyketal nanoparticle-mediated delivery of mature microRNAs. Biomaterials. 2013; 34:4235–41. [PubMed: 23489923]
6. Rogler CE, Levoci L, Ader T, Massimi A, Tchaikovskaya T, Norel R, et al. MicroRNA-23b cluster microRNAs regulate transforming growth factor-beta/bone morphogenetic protein signaling and liver stem cell differentiation by targeting Smads. Hepatology (Baltimore, Md). 2009; 50:575–84.
7. Suomi S, Taipaleenmaki H, Seppanen A, Ripatti T, Vaananen K, Hentunen T, et al. MicroRNAs regulate osteogenesis and chondrogenesis of mouse bone marrow stromal cells. Gene regulation and systems biology. 2008; 2:177–91. [PubMed: 19787082]
8. Ghildiyal M, Zamore PD. Small silencing RNAs: an expanding universe. Nature reviews Genetics. 2009; 10:94–108.
9. Lian JB, Stein GS, van Wijnen AJ, Stein JL, Hassan MQ, Gaur T, et al. MicroRNA control of bone formation and homeostasis. Nature reviews Endocrinology. 2012; 8:212–27.
10. Enerly E, Steinfeld I, Kleivi K, Leivonen SK, Aure MR, Russnes HG, et al. Correction: miRNA-mRNA Integrated Analysis Reveals Roles for miRNAs in Primary Breast Tumors. PloS one. 2013; 8
11. Huang Z, Huang D, Ni S, Peng Z, Sheng W, Du X. Plasma microRNAs are promising novel biomarkers for early detection of colorectal cancer. International journal of cancer. 2010; 127:118–26. [PubMed: 19876917]
12. Bartel DP. MicroRNAs: genomics, biogenesis, mechanism, and function. Cell. 2004; 116:281–97. [PubMed: 14744438]

13. Janssen HL, Reesink HW, Lawitz EJ, Zeuzem S, Rodriguez-Torres M, Patel K, et al. Treatment of HCV infection by targeting microRNA. The New England journal of medicine. 2013; 368:1685–94. [PubMed: 23534542]
14. Zhang J, Tu Q, Bonewald LF, He X, Stein G, Lian J, et al. Effects of miR-335-5p in modulating osteogenic differentiation by specifically downregulating Wnt antagonist DKK1. J Bone Miner Res. 2011; 26:1953–63. [PubMed: 21351149]
15. Zhang L, Tang Y, Zhu X, Tu T, Sui L, Han Q, et al. Overexpression of MiR-335-5p Promotes Bone Formation and Regeneration in Mice. J Bone Miner Res. 2017; 32:2466–75. [PubMed: 28846804]
16. Whitehead KA, Matthews J, Chang PH, Niroui F, Dorkin JR, Severgnini M, et al. In vitro-in vivo translation of lipid nanoparticles for hepatocellular siRNA delivery. ACS nano. 2012; 6:6922–9. [PubMed: 22770391]
17. Whitehead KA, Sahay G, Li GZ, Love KT, Alabi CA, Ma M, et al. Synergistic silencing: combinations of lipid-like materials for efficacious siRNA delivery. Molecular therapy : the journal of the American Society of Gene Therapy. 2011; 19:1688–94. [PubMed: 21750531]
18. Kanasty RL, Whitehead KA, Vegas AJ, Anderson DG. Action and reaction: the biological response to siRNA and its delivery vehicles. Molecular therapy : the journal of the American Society of Gene Therapy. 2012; 20:513–24. [PubMed: 22252451]
19. Novobrantseva TI, Borodovsky A, Wong J, Klebanov B, Zafari M, Yucius K, et al. Systemic RNAi-mediated Gene Silencing in Nonhuman Primate and Rodent Myeloid Cells. Molecular therapy Nucleic acids. 2012; 1:e4. [PubMed: 23344621]
20. Akinc A, Zumbuehl A, Goldberg M, Leshchiner ES, Busini V, Hossain N, et al. A combinatorial library of lipid-like materials for delivery of RNAi therapeutics. Nature biotechnology. 2008; 26:561–9.
21. Wang M, Sun S, Alberti KA, Xu Q. A combinatorial library of unsaturated lipidoids for efficient intracellular gene delivery. ACS synthetic biology. 2012; 1:403–7. [PubMed: 23651337]
22. Love KT, Mahon KP, Levins CG, Whitehead KA, Querbes W, Dorkin JR, et al. Lipid-like materials for low-dose, in vivo gene silencing. Proceedings of the National Academy of Sciences of the United States of America. 2010; 107:1864–9. [PubMed: 20080679]
23. Sun S, Wang M, Knupp SA, Soto-Feliciano Y, Hu X, Kaplan DL, et al. Combinatorial library of lipidoids for in vitro DNA delivery. Bioconjug Chem. 2012; 23:135–40. [PubMed: 22148515]
24. Akinc A, Goldberg M, Qin J, Dorkin JR, Gamba-Vitalo C, Maier M, et al. Development of lipidoid-siRNA formulations for systemic delivery to the liver. Molecular therapy : the journal of the American Society of Gene Therapy. 2009; 17:872–9. [PubMed: 19259063]
25. Wang M, Alberti K, Varone A, Pouli D, Georgakoudi I, Xu Q. Enhanced intracellular siRNA delivery using bioreducible lipid-like nanoparticles. Advanced healthcare materials. 2014; 3:1398–403. [PubMed: 24574196]
26. Sun S, Wang M, Alberti KA, Choy A, Xu Q. DOPE facilitates quaternized lipidoids (QLDs) for in vitro DNA delivery. Nanomedicine : nanotechnology, biology, and medicine. 2013; 9:849–54.
27. Tu Q, Valverde P, Li S, Zhang J, Yang P, Chen J. Osterix overexpression in mesenchymal stem cells stimulates healing of critical-sized defects in murine calvarial bone. Tissue Eng. 2007; 13:2431–40. [PubMed: 17630878]
28. Yu L, Tu Q, Han Q, Zhang L, Sui L, Zheng L, et al. Adiponectin regulates bone marrow mesenchymal stem cell niche through a unique signal transduction pathway: an approach for treating bone disease in diabetes. Stem Cells. 2015; 33:240–52. [PubMed: 25187480]
29. Valverde P, Tu Q, Chen J. BSP and RANKL induce osteoclastogenesis and bone resorption synergistically. J Bone Miner Res. 2005; 20:1669–79. [PubMed: 16059638]
30. Wu Y, Tu Q, Valverde P, Zhang J, Murray D, Dong LQ, et al. Central adiponectin administration reveals new regulatory mechanisms of bone metabolism in mice. Am J Physiol Endocrinol Metab. 2014; 306:E1418–30. [PubMed: 24780611]
31. Valverde P, Zhang J, Fix A, Zhu J, Ma W, Tu Q, et al. Overexpression of bone sialoprotein leads to an uncoupling of bone formation and bone resorption in mice. J Bone Miner Res. 2008; 23:1775–88. [PubMed: 18597627]

32. Takeda YS, Wang M, Deng P, Xu Q. Synthetic bioreducible lipid-based nanoparticles for miRNA delivery to mesenchymal stem cells to induce neuronal differentiation. Bioeng Transl Med. 2016; 1:160–7. [PubMed: 29313011]

33. Felgner JH, Kumar R, Sridhar CN, Wheeler CJ, Tsai YJ, Border R, et al. Enhanced gene delivery and mechanism studies with a novel series of cationic lipid formulations. The Journal of biological chemistry. 1994; 269:2550–61. [PubMed: 8300583]

34. Liu X, Ma PX. Polymeric scaffolds for bone tissue engineering. Annals of biomedical engineering. 2004; 32:477–86. [PubMed: 15095822]

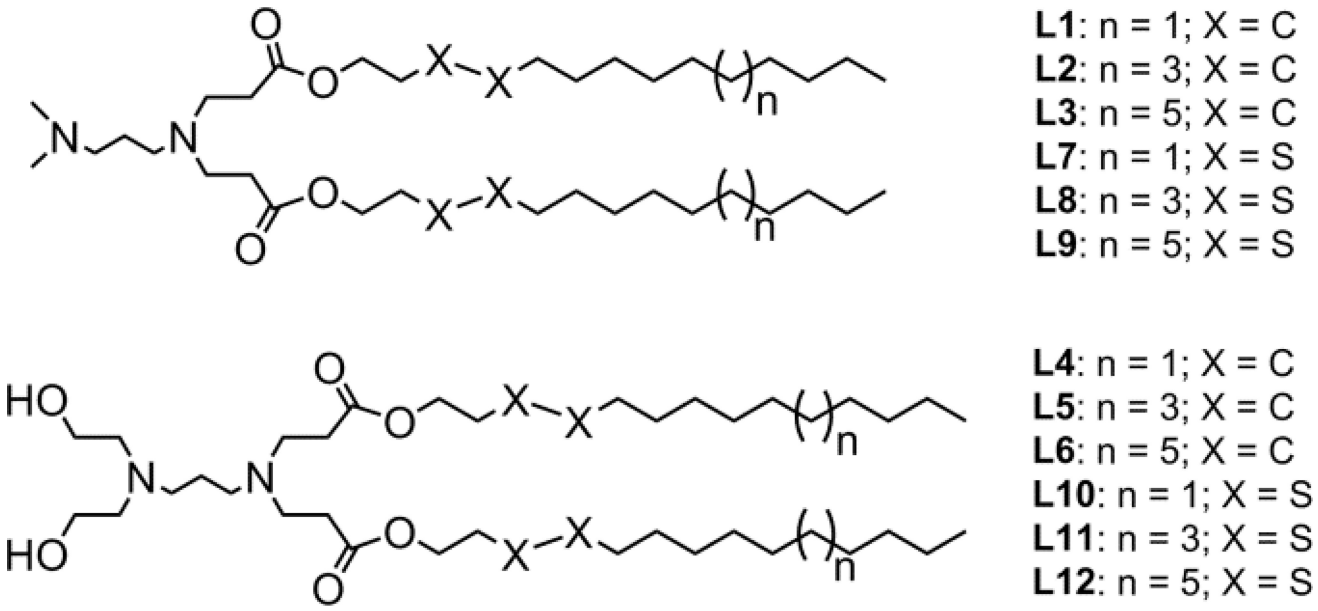

Figure 1. Chemical structure of lipidoids L1 to L12

Lipidoids were prepared by heating commercially available amines with lipophilic acrylates, without solvent or catalysts as previously described [25, 26]. We formulated lipidoid nanoparticles for miRNA delivery, by mixing lipidoids, cholesterol, and 1, 2-dioleoyl-*sn*-glycero-3-phosphoethanolamine (DOPE) [25, 26].

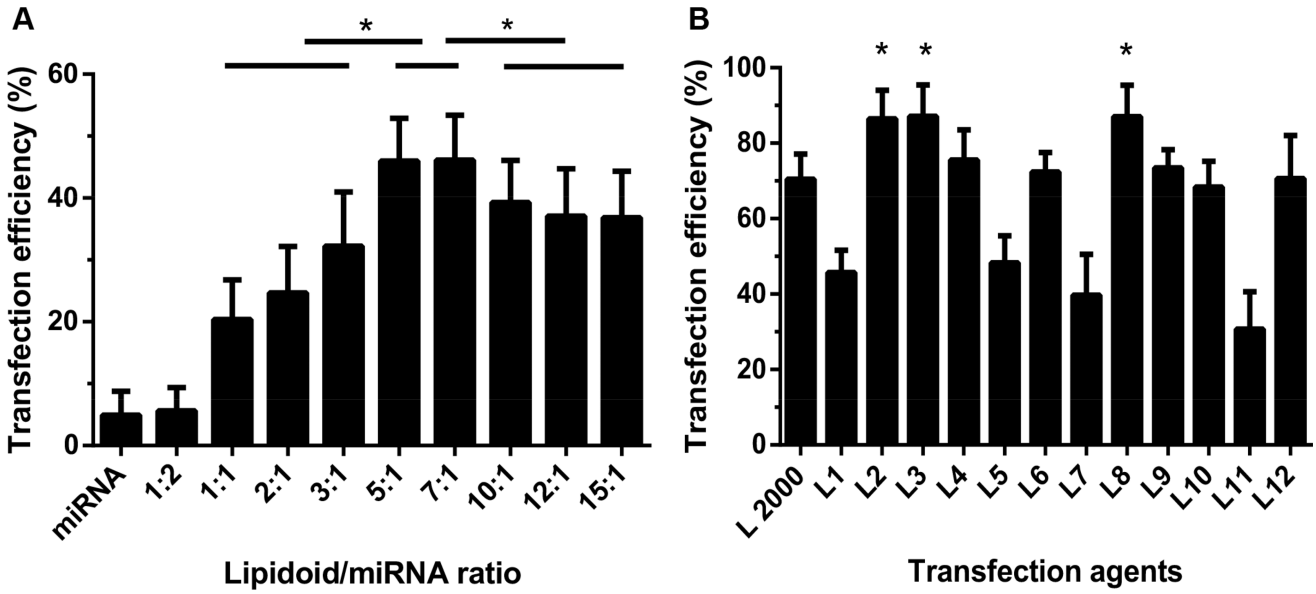

Figure 2. Optimal lipidoid/miRNA ratio determination and *in vitro* transfection efficiency screening of L1 to L12 lipidoids

(A) LMFs were generated with lipidoid L1 and Cy3-labeled miRNA at different lipidoid/miRNA ratios to identify optimal lipidoid/miRNA weight ratio via flow cytometry analysis (n = 3). (B) Transfection efficiency of LMFs developed with lipidoids L1 to L12 and Cy3-labeled Cy3-labeled miRNA at lipidoid/miRNA ratio of 5:1 were compared with commercially available transfection reagent Lipofectamine 2000 (n = 3).

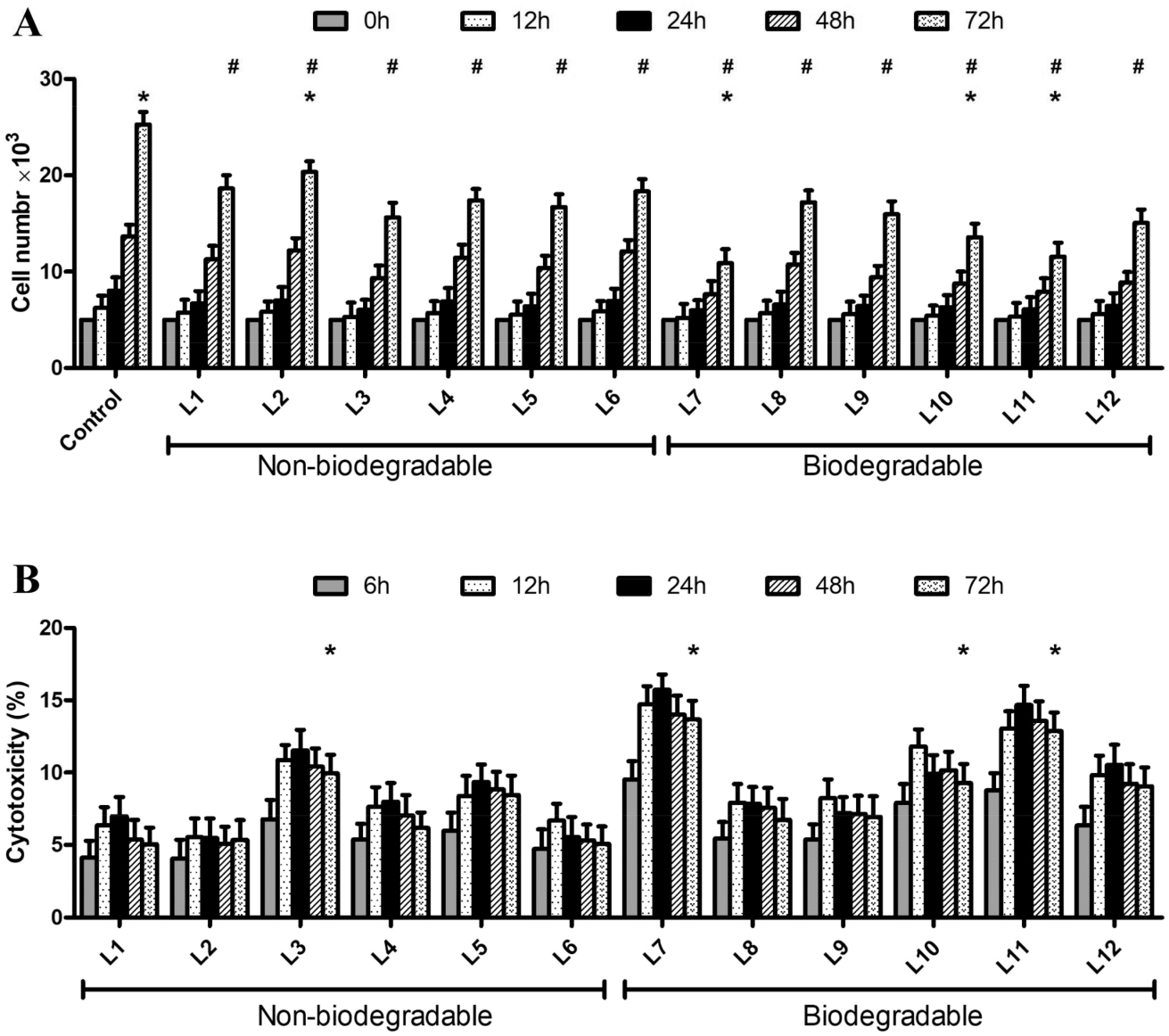

Figure 3. Influence of LMFs on cell proliferation and Cytotoxicity of LMFs

A. Proliferation of C3H10T1/2 cells transfected with LMFs was determined using the CCK-8 assay. Results were normalized with the ones of non-transfected cells used as negative controls. P<0.05, # versus control (0 h), * versus L8. B. C3H10T1/2 cells were treated with LMFs for 6, 12, 24, 48 and 72h, and released LDH was measured and normalized. *P<0.05, versus control (6 h).

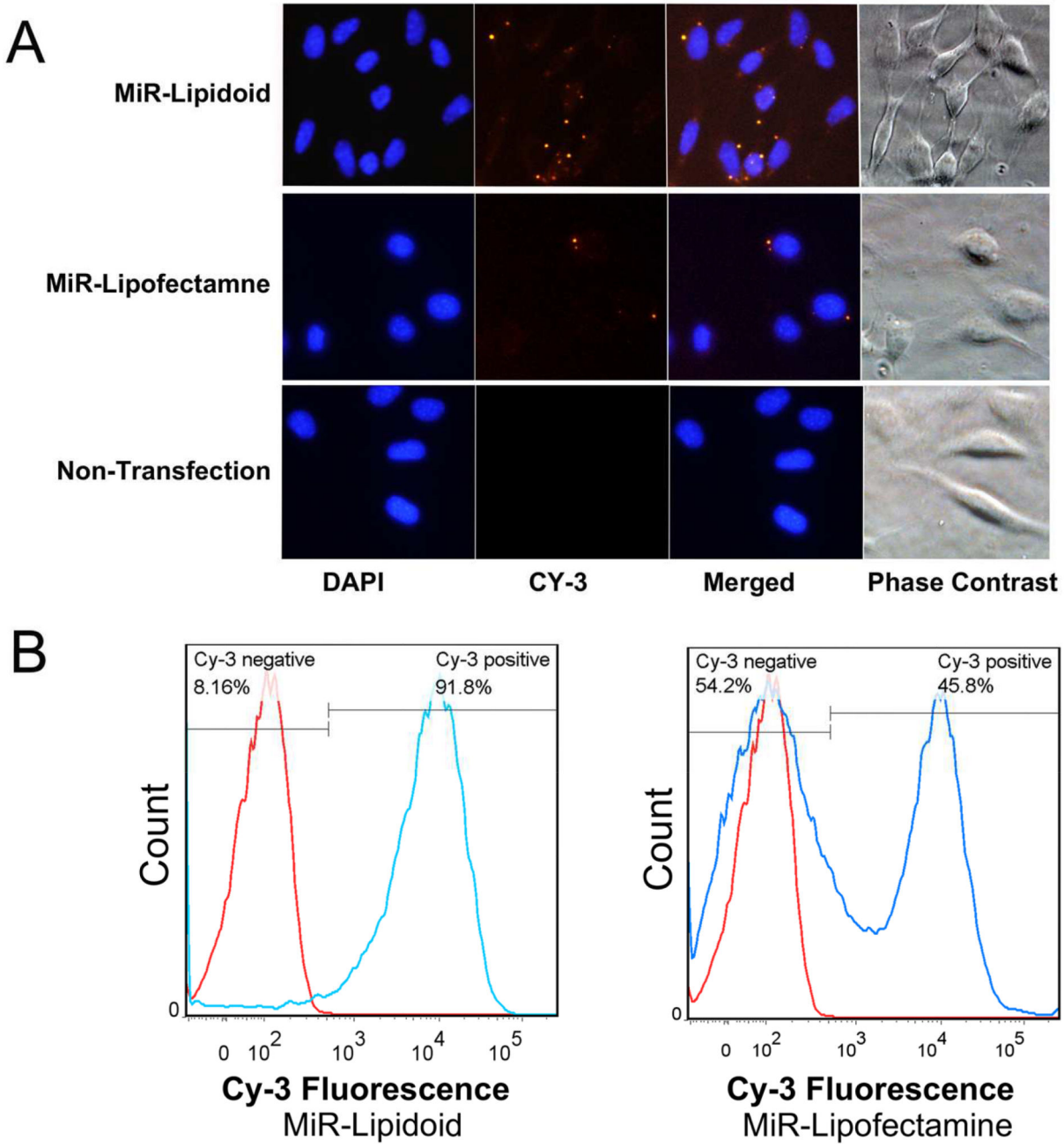

Figure 4. Internalization of LMFs in C3H10T1/2 cells

A. Cells were transfected with Cy-3 labeled miRNA formulated with L8 or Lipofectamine 2000 for 6 hours and compared with non-transfected cells. Cells were fixed with 4% paraformaldehyde and nuclei were stained with DAPI (blue). Bright yellow fluorescence resulted from delivery of cy3-labelled miRNA-loaded in lipidoids and merged images of cy3 and DAPI were obtained. Fluorescence images of transfected cells were recorded using a system microscope (OLYMPUS BX53): 40× objective, excitation wavelength 550nm and cy3 filter set (Semrock Cy3-4040C-OFF). Images of 400× were acquired with the same acquisition parameters. Images from phase contrast field were used to determne the

localization of fluorescence. B. Flow cytometry analysis to compare the transfection efficacy of LMF formulations with Lipofectamine 2000 in C3H10T1/2 cultures. Red line, non-trasfection negative control groups; Blue line, Lipidoid or Lipofectamine transfection groups.

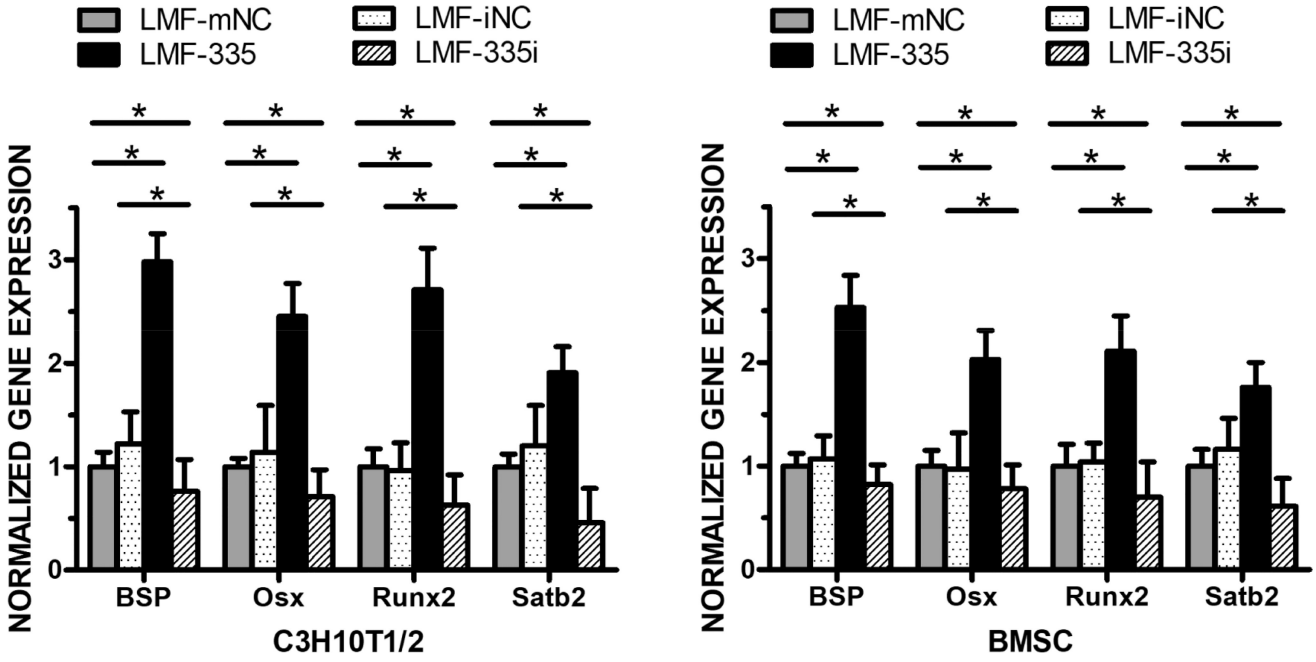

Figure 5. LMFs induction of osteogenic gene expression *in vitro*

qRT-PCR showed mRNA expression changes of osteogenic genes, including BSP, Osx, Runx2, and Satb2. LMF-335 could upregulate the gene expression of all these bone markers, while knockdown endogenous miRNA335 using LMF-335i downregulated the expression of bone markers in C3H10T-1/2 cells (A) and BMSCs (B). Three independent experiments were performed in triplicate, and data are represented as mean±SD. *$p<0.05$. NC=negative control.

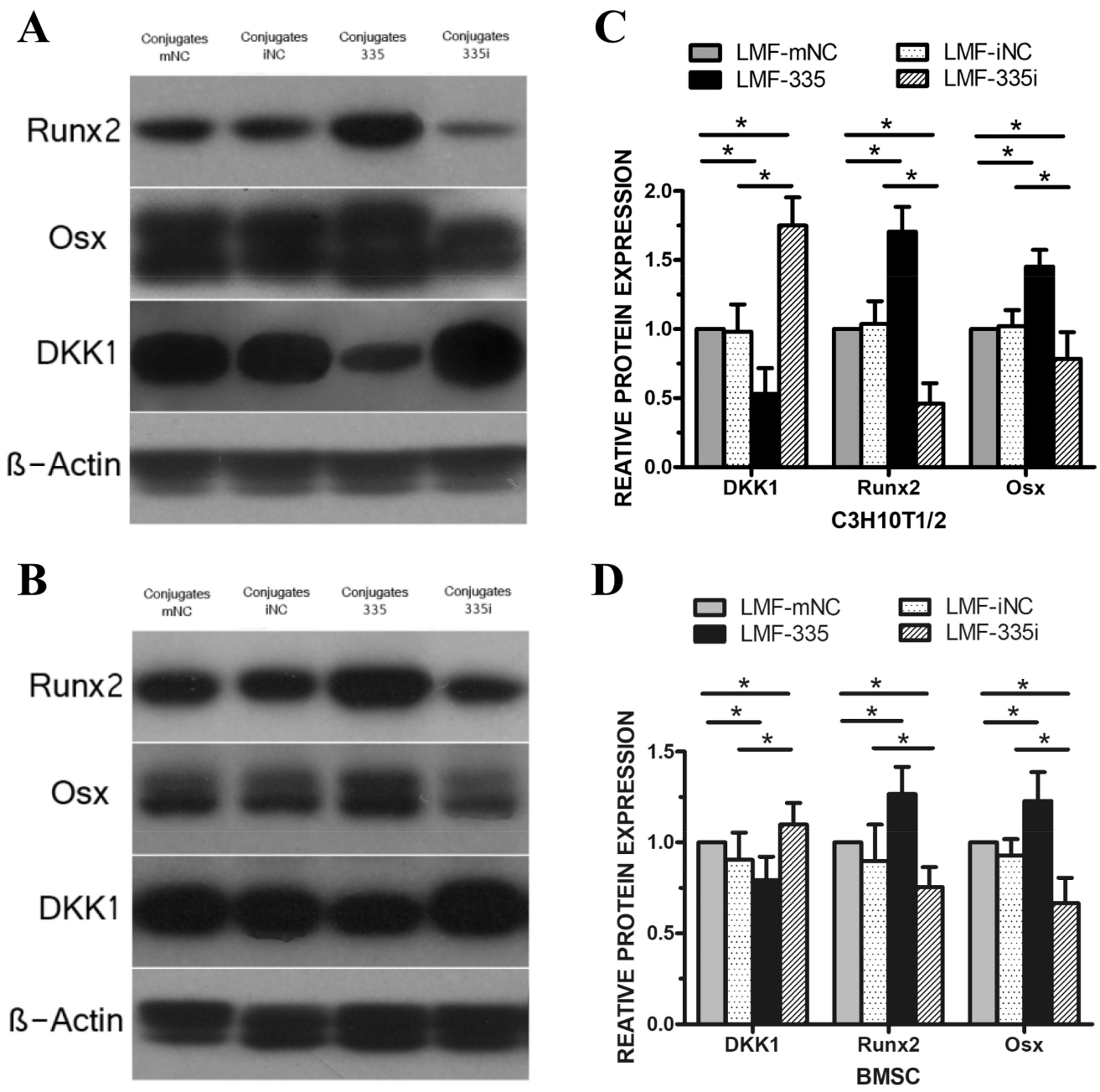

Figure 6. LMFs upregulated protein expression of osteogenic transcription factors

Western blot revealed increased production of osteogenic transcription factors, Osx and Runx-2 after transfected with the LMF-335 in C3H10T-1/2 cells, which could be considered the result of decreased protein expression level of DKK1, an inhibitor of Wnt signal pathway (A, C). The relative density of the bands was normalized to beta-actin and then to the control groups in BMSCs (B, D). Measurements were performed in triplicate, and data are represented as mean±SD. *p<0.05. NC=negative control.

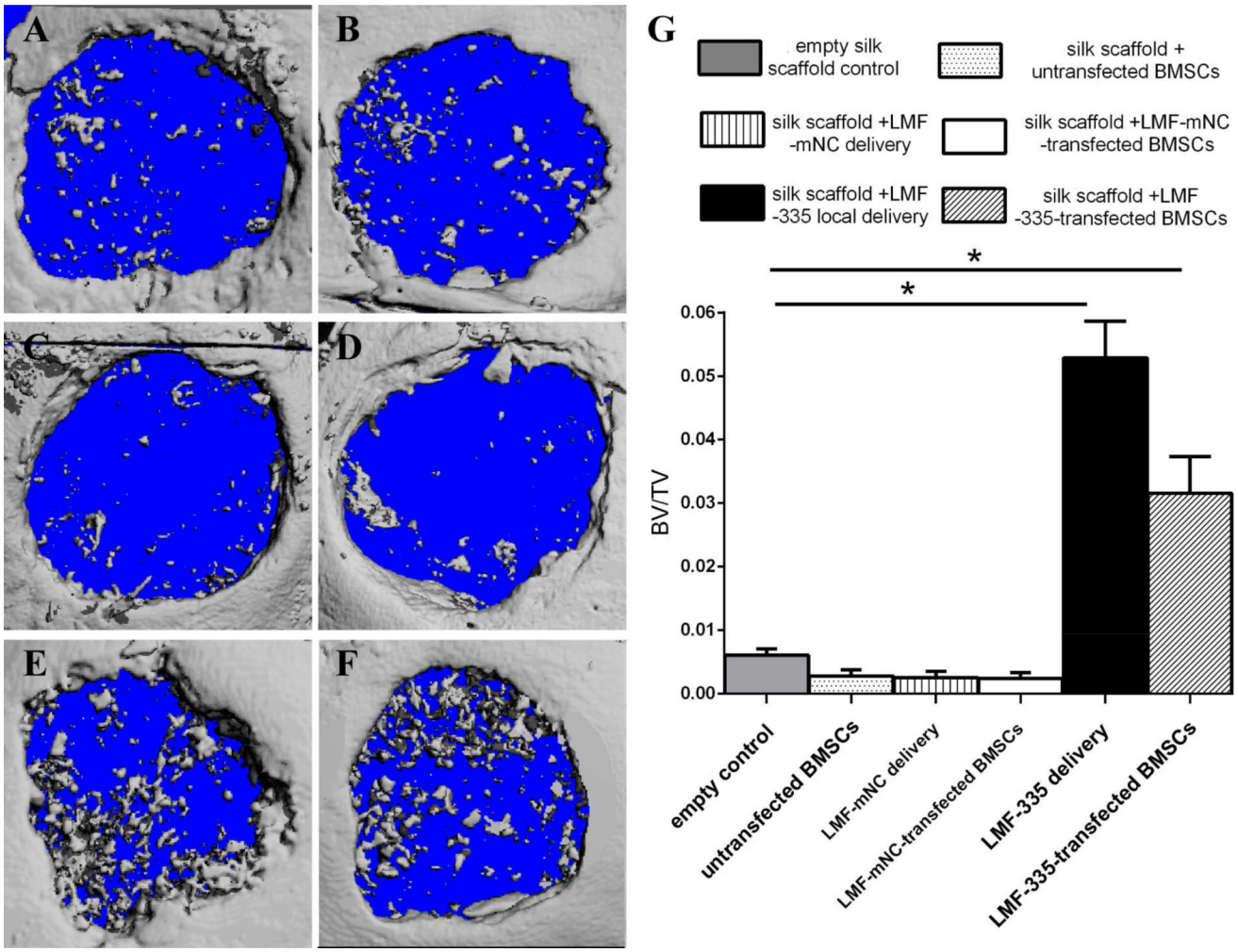

Figure 7. MicroCT analysis of LMF-335 induced calvarial bone healing

MicroCT was utilized to evaluate new bone formation of calvarial bone defects 5 weeks after surgery (n=3 mice per group). Groups evaluated included: A: Silk scaffold empty control; B: silk scaffold + untransfected BMSCs; C: silk scaffold + LMF-mNC local delivery; D: silk scaffold + LMF-mNC-untransfected BMSCs.; E: silk scaffold + LMF-335 local delivery; F: silk scaffold + LMF-335-transfected BMSCs. G. BV/TV quantification analysis (*$p<0.05$).

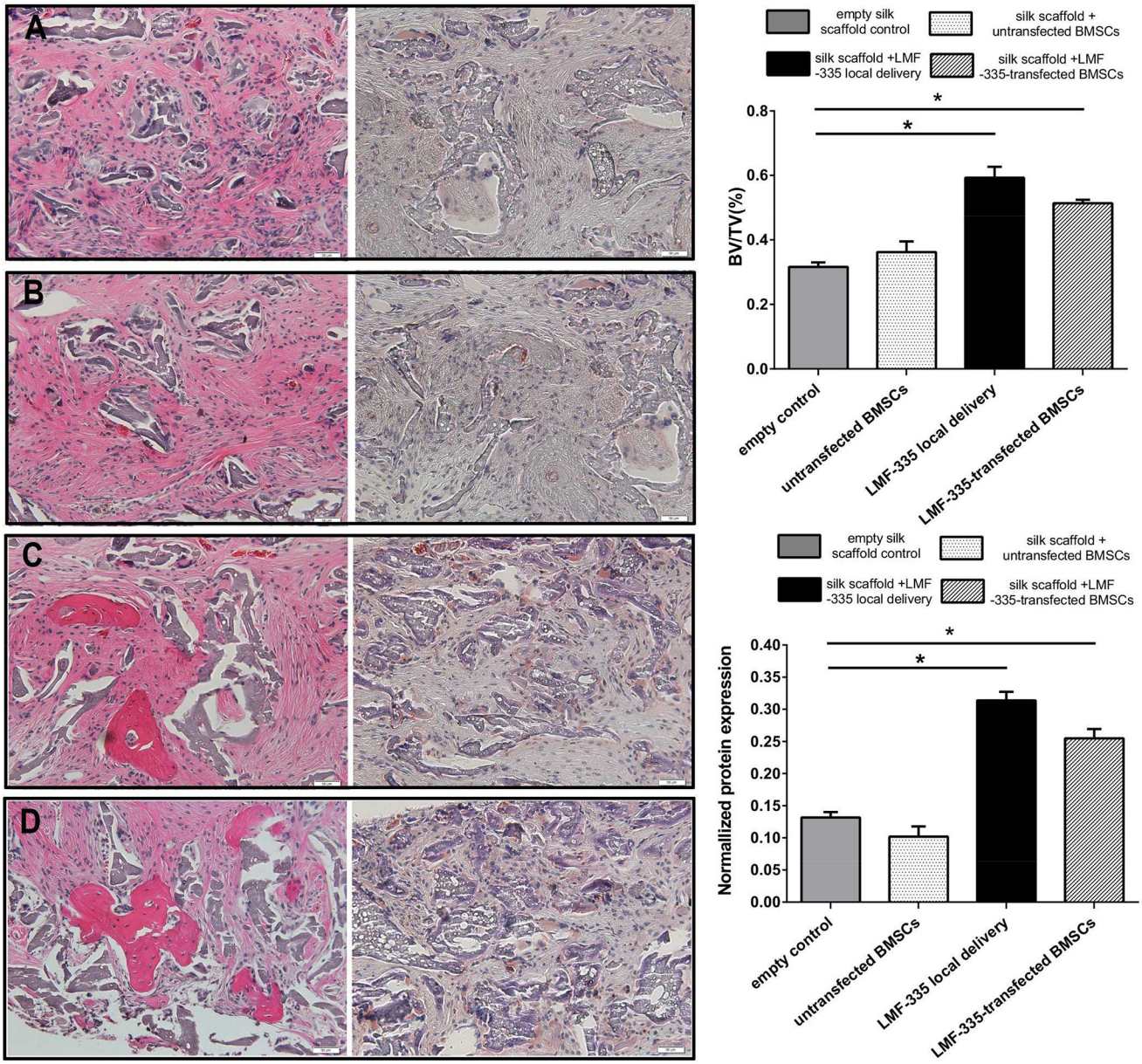

Figure 8. HE and OCN IHC analysis of regenerated bone defects by LMF-335

New bone formation areas were identified and quantified by HE staining (shown on the left) and OCN IHC staining (shown on the right). A: empty silk scaffold control; B: silk scaffold + untransfected BMSCs; C: silk scaffold + LMF-335 local delivery; D: silk scaffold + LMF-335-transfected BMSCs. Quantification of new bone formation and normalized OCN expression are represented by bar graphs. (*$p<0.05$).

Table1

Sequences of primers for qRT-PCR

Primer	Sequence
BSP	Forward: 5’-GAC TTT TGA GTT AGC GGC ACT-3’
	Reverse: 5’-CCG CCA GCT CGT TTT CAT C-3’
OSX	Forward: 5’-ATGGCGTCCTCTCTGCTTG-3’
	Reverse: 5’-TGAAAGGTCAGCGTATGGCTT-3’
Runx2	Forward: 5’-AAC GAT CTG AGA TTT GTG GGC-3’
	Reverse: 5’-CCT GCG TGG GAT TTC TTG GTT-3’
Satb2	Forward: 5’-AGG CCC AAG GAA TAA TCA AGC-3’
	Reverse: 5’-GCG TCA CAA CGT GAT AGA CAT C-3’
GAPDH	Forward: 5’-AGG TCG GTG TGA ACG GAT TTG-3’
	Reverse: 5’-TGT AGA CCA TGT AGT TGA GGT CA-3’